# The Star Formation Newsletter

A community newsletter on Star and Planet Formation research

**No. 345** — 26 September 2021
Editor: João Alves www.starformation.news

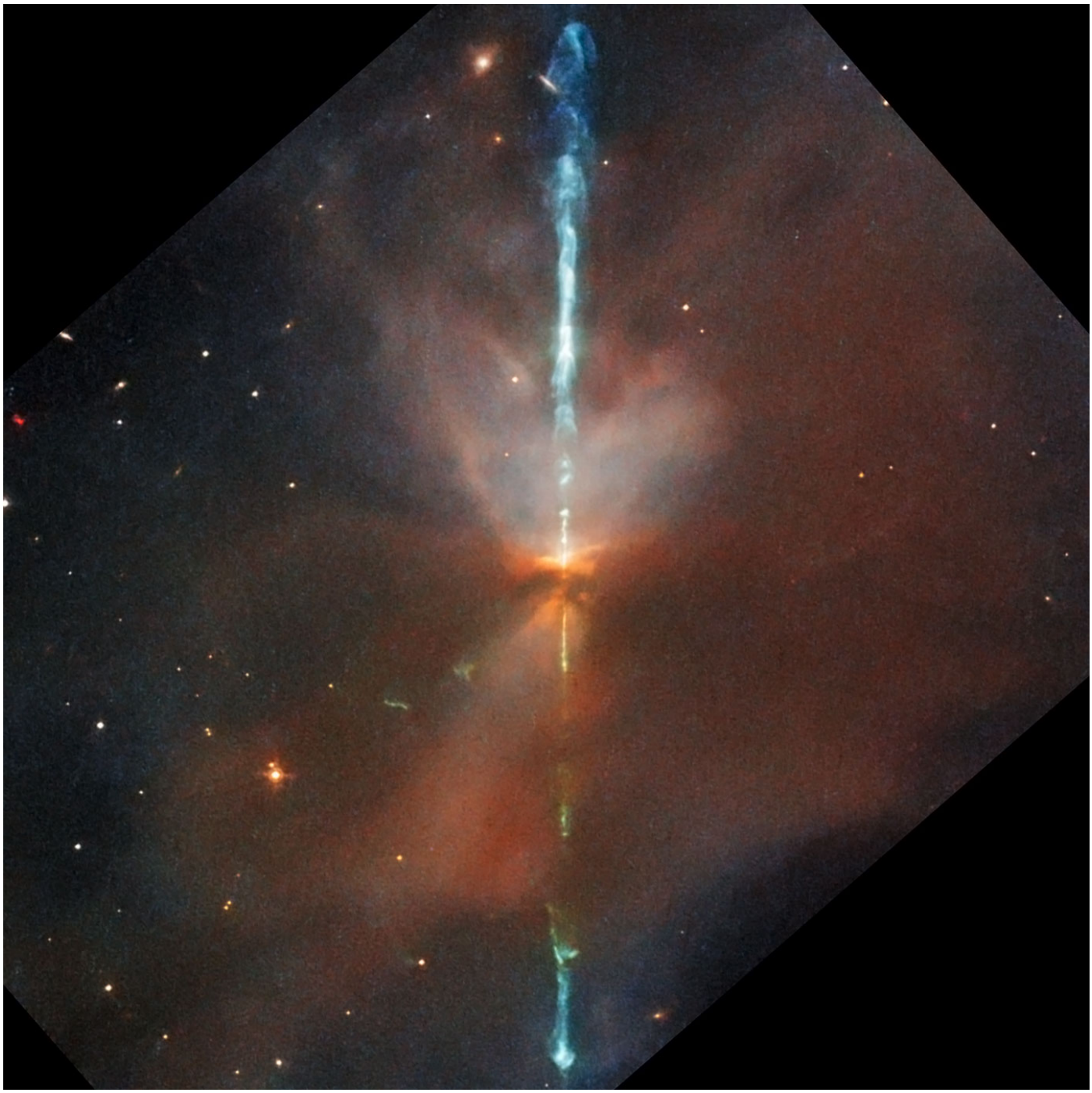

**Links to sections**


| | | | | |
|---|---|---|---|---|
| Interviews | Reviews | Perspective | Favorite objects | Archive |
| Meetings | Jobs | New PhDs | Announcements | Books |


**Cover image caption**

Spectacular image of Herbig–Haro object HH111, imaged by Hubble's Wide Field Camera 3 (WFC3). HH111 lives in L1617, one of a series of finger-like clouds next to the better studies L1622. Newly formed stars expel very narrow jets of rapidly moving ionised gas that collide with the gas and dust surrounding newly-formed stars at speeds of hundreds of kilometres per second. It is these energetic collisions that create Herbig–Haro objects such as HH111. Credit: ESA/Hubble & NASA, B. Nisini.

**Note from the Editor**

The Star Formation Newsletter is now on the web at **www.starformation.news**. This PDF file contains the monthly Abstracts and links to the different Newsletter sections. Red text in this PDF is a url link. Submitting an abstract to the SFN is as simple as entering the arXiv ID (e.g., 2006.10139) in a web form on the SFN web site. **Do not remove the LaTeX formatting when submitting to the arXiv**. If you do, your abstract will not look great either at the arXiv (which uses MathJax to convert LaTeX math symbols to the web) or the SFN.

# Abstracts

## 1. An ALMA study of hub-filament systems I. On the clump mass concentration within the most massive cores

**Michael Anderson, Nicolas Peretto, Sarah E. Ragan, Andrew J. Rigby, Adam Avison, Ana Duarte-Cabral, Gary A. Fuller, Yancy L. Shirley, Alessio Traficante, Gwenllian M. Williams** ★ The physical processes behind the transfer of mass from parsec-scale clumps to massive-star-forming cores remain elusive. We investigate the relation between the clump morphology and the mass fraction that ends up in its most massive core (MMC) as a function of infrared brightness, i.e. a clump evolutionary tracer. Using ALMA 12 m and ACA we surveyed 6 infrared-dark hubs in 2.9mm continuum at ∼3" resolution. To put our sample into context, we also re-analysed published ALMA data from a sample of 29 high mass-surface density ATLASGAL sources. We characterise the size, mass, morphology, and infrared brightness of the clumps using Herschel and Spitzer data. Within the 6 newly observed hubs, we identify 67 cores, and find that the MMCs have masses between 15-911 $M_\odot$ within a radius of 0.018-0.156 pc. The MMC of each hub contains 3-24% of the clump mass ($f_{\rm MMC}$), becoming 5-36% once core masses are normalised to the median core radius. Across the 35 clumps, we find no significant difference in the median $f_{\rm MMC}$ values of hub and non-hub systems, likely the consequence of a sample bias. However, we find that $f_{\rm MMC}$ is ∼7.9 times larger for infrared-dark clumps compared to infrared-bright ones. This factor increases up to ∼14.5 when comparing our sample of 6 infrared-dark hubs to infrared-bright clumps. We speculate that hub-filament systems efficiently concentrate mass within their MMC early on during its evolution. As clumps evolve, they grow in mass, but such growth does not lead to the formation of more massive MMCs.

## 2. Long-term stability of planets in and around binary stars

**Harry A. Ballantyne, Tore Espaas, Bethan Z. Norgrove, Bethany A. Wootton, Benjamin R. Harris, Isaac L. Pepper, Richard D. Smith, Rosie E. Dommett, Richard J. Parker** ★ Planets are observed to orbit the component star(s) of stellar binary systems on so-called circumprimary or circumsecondary orbits, as well as around the entire binary system on so-called circumbinary orbits. Depending on the orbital parameters of the binary system a planet will be dynamically stable if it orbits within some critical separation of the semimajor axis in the circumprimary case, or beyond some critical separation for the circumbinary case. We present N-body simulations of star-forming regions that contain populations of primordial binaries to determine the fraction of binary systems that can host stable planets at various semimajor axes, and how this fraction of stable systems evolves over time. Dynamical encounters in star-forming regions can alter the orbits of some binary systems, which can induce long-term dynamical instabilities in the planetary system and can even change the size of the habitable zone(s) of the component stars. However, the overall fraction of binaries that can host stable planetary systems is not greatly affected by either the assumed binary population, or the density of the star-forming region. Instead, the critical factor in determining

how many stable planetary systems exist in the Galaxy is the stellar binary fraction - the more stars that are born as singles in stellar nurseries, the higher the fraction of stable planetary systems.

## 3. A search for transiting companions in the J1407 (V1400 Cen) system

**S. Barmentloo, C. Dik, M. A. Kenworthy, E. E. Mamajek, F. -J. Hambsch, D. E. Reichart, J. E. Rodriguez, D. M. van Dam** ★ In 2007, the young star 1SWASP J140747.93-394542.6 (V1400 Cen) underwent a complex series of deep eclipses over 56 days. This was attributed to the transit of a ring system filling a large fraction of the Hill sphere of an unseen substellar companion. Subsequent photometric monitoring has not found any other deep transits from this candidate ring system, but if there are more substellar companions and they are coplanar with the potential ring system, there is a chance that they will transit the star as well. This young star is active and the light curves show a 5% modulation in amplitude with a dominant rotation period of 3.2 days due to star spots rotating in and out of view. We model and remove the rotational modulation of the J1407 light curve and search for additional transit signatures of substellar companions orbiting around J1407. We combine the photometry of J1407 from several observatories, spanning a 19 year baseline. We remove the rotational modulation by modeling the variability as a periodic signal, whose periodicity changes slowly with time over several years due to the activity cycle of the star. A Transit Least Squares (TLS) analysis searches for any periodic transiting signals within the cleaned light curve. We identify an activity cycle of J1407 with a period of 5.4 years. A Transit Least Squares search does not find any plausible periodic eclipses in the light curve, from 1.2% amplitude at 5 days up to 1.9% at 20 days. This sensitivity is confirmed by injecting artificial transits into the light curve and determining the recovery fraction as a function of transit depth and orbital period. J1407 is confirmed as a young active star with an activity cycle consistent with a rapidly rotating solar mass star. With the rotational modulation removed, the TLS analysis rules out transiting companions with radii larger than about 1 Jupiter.

## 4. Structured velocity field in the inner envelope of B335: ALMA observations of rare CO isotopologues

**Victoria Cabedo, Anaëlle Maury, Josep Miquel Girart, Marco Padovani** ★ Studying Class 0 objects is very important, as it allows to characterize dynamical processes at the onset of the star formation process, and to determine the physical mechanisms responsible for the outcome of the collapse. Observations of dense gas tracers allow the characterization of key kinematics of the gas directly involved in the star-formation process, such as infall, outflow or rotation. This work aims at investigating the molecular line velocity profiles of the Class 0 protostellar object B335 and attempts to put constraints on the infall motions happening in the circumstellar gas of the object. Observations of $C^{17}O$ (1-0), $C^{18}O$ (1-0) and $^{12}CO$ (2-1) transitions are presented and the spectral profiles are analyzed at envelope radii between 100 and 860 au. $C^{17}O$ emission presents a double peaked line profile distributed in a complex velocity field. Both peaks present an offset of 0.2 to 1 km $s^{-1}$ from the systemic velocity of the source in the probed area. The optical depth of the $C^{17}O$ emission has been estimated and found to be less than 1, suggesting that the two velocity peaks trace two distinct velocity components of the gas in the inner envelope. After discarding possible motions that could produce the complex velocity pattern, such as rotation and outflow, it is concluded that infall is producing the velocity field. Because inside-out symmetric collapse cannot explain those observed profiles, it is suggested that those are produced by non-isotropic accretion from the envelope into the central source along the outflow cavity walls.

## 5. The SVS13-A Class I chemical complexity as revealed by S-bearing species. SOLIS XIII

**C. Codella, E. Bianchi, L. Podio, S. Mercimek, C. Ceccarelli, A. Lopez-Sepulcre, R. Bachiller, P. Caselli, N. Sakai, R. Neri, F. Fontani, C. Favre, N. Balucani, B. Lefloch, S. Viti, S. Yamamoto** ★ Aims: The goal is to obtain a census of S-bearing species using interferometric images, towards SVS13-A, a Class I object associated with a hot corino rich in interstellar complex organic molecules. Methods: We used data at 3mm and 1.4mm obtained with IRAM-NOEMA in the framework of the Large Program SOLIS. Results: We imaged the spatial distribution of the line emission of 32SO, 34SO, C32S, C34S, C33S, OCS, H2C32S, H2C34S, and NS. The low excitation (9 K) 32SO line is tracing the fast collimated jet driven by the nearby SVS13-B. Conversely, the rest of the lines are confined in the inner SVS13-A region, where complex organics have been previously imaged. The non-LTE LVG analysis of SO, SO2, and H2CS indicates a hot corino origin (60-120 au). Temperatures between 50 K and 300 K, and volume densities larger than $10^5$ cm-3 have been derived. The abundances are in the following ranges: 0.3-6 $10^{-}6$ (CS), 7 $10^{-}9$ - 1 $10^{-}7$ (SO), 1-10 $10^{-}7$ (SO2), a few $10^{-}10$ (H2CS and OCS), and $10^{-10}$ - $10^{-9}$(NS). The N(NS)/N($NS^+$) ratio is larger than 10, supporting that the $NS^+$ ion is mainly formed in the extended envelope. Conclusions: The [H2CS]/[H2CO] ratio increases with time (from Class 0 to Class II objects) by more than one order of magnitude. This suggests that [S]/[O] changes along the Sun-like star forming process. The estimate of the [S]/[H] budget in SVS13-A is 2%-17% of the Solar System value (1.8 $10^{-}5$), being consistent with what was previously measured towards Class 0 objects (1%-8%).

This supports that the enrichment of the sulphuretted species with respect to dark clouds keeps constant from the Class 0 to the Class I stages of low-mass star formation. The present findings stress the importance of investigating the chemistry of star forming regions using large observational surveys as well as sampling regions on a Solar System scale.

## 6. The GRAVITY Young Stellar Object survey VIII. Gas and dust faint inner rings in the hybrid disk of HD141569

**GRAVITY Collaboration, V. Ganci et al.** ★ The formation and evolution of planetary systems impact the primordial accretion disk. HD141569 is the only known pre-main sequence star characterized by a hybrid disk. Observations probed the outer-disk structure showing a complex system of rings and interferometric observations attempted to characterize its inner 5 au region, but derived limited constraints. The goal of this work was to explore with new high-resolution interferometric observations the properties of the dust and gas in the internal regions of HD141569. We observed HD141569 on mas scales with GRAVITY/VLTI in the near-infrared at low and high spectral resolution. We interpreted the visibilities and spectral energy distribution with geometrical models and radiative transfer techniques to constrain the dust emission. We analyzed the high spectral resolution quantities to investigate the properties of the Br-Gamma line emitting region. Thanks to the combination of three different epochs, GRAVITY resolves the inner dusty disk in the K band. Data modeling shows that an IR excess of about 6% is spatially resolved and that the origin of this emission is confined in a ring of material located at a radius of 1 au from the star with a width smaller than 0.3 au. The MCMax modeling suggests that this emission could originate from a small amount of QHPs, while large silicate grain models cannot reproduce at the same time the observational constraints on the properties of near-IR and mid-IR fluxes. The differential phases in the Br-Gamma line clearly show an S-shape that can be best reproduced witha gas disk in Keplerian rotation, confined within 0.09 au. This is also hinted at by the double-peaked Br-Gamma emission line shape. The modeling of the continuum and gas emission shows that the inclination and position angle of these two components are consistent with a system showing relatively coplanar rings on all scales.

## 7. Measuring the Density Structure of an Accretion Hot Spot

**C. C. Espaillat, C. E. Robinson, M. M. Romanova, T. Thanathibodee, J. Wendeborn, N. Calvet, M. Reynolds, J. Muzerolle** ★ Magnetospheric accretion models predict that matter from protoplanetary disks accretes onto the star via funnel flows which follow the stellar field lines and shock on the stellar surface leaving a hot spot with a density gradient. Previous work has inferred different densities in the hot spot, but has not been sensitive to the radial density distribution. Attempts have been made to measure this with X-ray observations, but X-ray emission only traces a fraction of the hot spot and also coronal emission. Here we report periodic ultraviolet and optical light curves of the accreting star GM Aur that display a time lag of about 1 day between their peaks. The periodicity arises as the source of the ultraviolet and optical emission moves into and out of view as it rotates along with the star. The time-lag indicates a difference in the spatial distribution of ultraviolet and optical brightness over the stellar surface. Within the framework of the magnetospheric accretion model, this indicates a radial density gradient in a hot spot on the stellar surface since different density parts of the hot spot are expected to emit radiation at different wavelengths. These results are the first observational confirmation of the magnetospheric accretion model's prediction of a density gradient in the hot spot and demonstrate the insights gained from focusing on the wavelengths where the bulk of the accretion energy can be observed.

## 8. A Solar System formation analogue in the Ophiuchus star-forming complex

**John C. Forbes, João Alves, Douglas N. C. Lin** ★ Anomalies among the daughter nuclei of the extinct short-lived radionuclides (SLRs) in the calcium-aluminum-rich inclusions (CAIs) indicate that the Solar System must have been born near a source of the SLRs so that they could be incorporated before they decayed away. $\gamma$-rays from one such living SLR, $^{26}$Al, are detected in only a few nearby star-forming regions. Here we employ multi-wavelength observations to demonstrate that one such region, Ophiuchus, containing many pre-stellar cores that may serve as analogs for the emerging Solar System, is inundated with $^{26}$Al from the neighboring Upper-Scorpius association, and so may provide concrete guidance for how SLR enrichment proceeded in the Solar System complementary to the meteoritics. We demonstrate via Bayesian forward modeling drawing on a wide range of observational and theoretical results that this $^{26}$Al likely 1) arises from supernova explosions, 2) arises from multiple stars, 3) has enriched the gas prior to the formation of the cores, and 4) gives rise to a broad distribution of core enrichment spanning about two orders of

magnitude. This means that if the spread in CAI ages is small, as it is in the Solar System, protoplanetary disks must suffer a global heating event.

## 9. PENELLOPE II. CVSO 104: a pre-main sequence close binary with an optical companion in Ori OB1

**A. Frasca, H. M. J. Boffin, C. F. Manara, J. M. Alcalá, P. Ábrahám, E. Covino, M. Fang, M. Gangi, G. J. Herczeg, Á. Kóspál, L. Venuti, F. M. Walter, J. Alonso-Santiago, K. Grankin, M. Siwak, E. Alecian, S. Cabrit** ★ We present results of our study of the close pre-main sequence spectroscopic binary CVSO 104 in Ori OB1, based on data obtained within the PENELLOPE legacy program. We derive, for the first time, the orbital elements of the system and the stellar parameters of the two components. The system is composed of two early M-type stars and has an orbital period of about 5 days and a mass ratio of 0.92, but contrarily to expectations does not appear to have a tertiary companion. Both components have been (quasi-)synchronized, but the orbit is still very eccentric. The spectral energy distribution clearly displays a significant infrared excess compatible with a circumbinary disk. The analysis of HeI and Balmer line profiles, after the removal of the composite photospheric spectrum, reveals that both components are accreting at a similar level. We also observe excess emission in H$\alpha$ and H$\beta$, which appears redshifted or blueshifted by more than 100 km/s with respect to the mass center of the system depending on the orbital phase. This additional emission could be connected with accretion structures, such as funnels of matter from the circumbinary disk. We also analyze the optical companion located at about 2".4 from the spectroscopic binary. This companion, that we named CVSO 104B, turns out to be a background Sun-like star not physically associated with the PMS system and not belonging to Ori OB1.

## 10. Modeling accretion shocks at the disk-envelope interface – Sulfur chemistry

**M. L. van Gelder, B. Tabone, E. F. van Dishoeck, B. Godard** ★ As material from an infalling protostellar envelope hits the forming disk, an accretion shock may develop which could (partially) alter the envelope material entering the disk. Observations with the Atacama Large Millimeter/submillimeter Array (ALMA) indicate that emission originating from warm SO and $SO_2$ might be good tracers of such accretion shocks. The goal of this work is to test under what shock conditions the abundances of gas-phase SO and $SO_2$ increase in an accretion shock at the disk-envelope interface. Detailed shock models including gas dynamics are computed using the Paris-Durham shock code for non-magnetized J-type accretion shocks in typical inner envelope conditions. The effect of pre-shock density, shock velocity, and strength of the ultraviolet (UV) radiation field on the abundance of warm SO and $SO_2$ is explored. Warm gas-phase chemistry is efficient in forming SO under most J-type shock conditions considered. In lower-velocity ( 3 km/s) shocks, the abundance of SO is increased through subsequent reactions starting from thermally desorbed $CH_4$ toward $H_2CO$ and finally SO. In higher velocity (>4 km/s) shocks, both SO and $SO_2$ are formed through reactions of OH and atomic S. The strength of the UV radiation field is crucial for SO and in particular $SO_2$ formation through the photodissociation of $H_2O$. Thermal desorption of SO and $SO_2$ ice is only relevant in high-velocity (>5 km/s) shocks at high densities ($> 10^7$ cm$^{-3}$). Warm emission from SO and $SO_2$ is a possible tracer of accretion shocks at the disk-envelope interface as long as a local UV field is present. Additional observations with ALMA at high-angular resolution could provide further constraints. Moreover, the James Webb Space Telescope will give access to other possible slow, dense shock tracers such as $H_2$, $H_2O$, and [S I] 25$\mu$m.

## 11. Comparing the spatial and kinematic distribution of gas and young stars around the shell-like structure in the CMa OB1 association

**Jane Gregorio-Hetem, Bertrand Lefloch, Annibal Hetem, Thierry Montmerle, Beatriz Fernandes, Edgar F. Mendoza, Marta De Simone** ★ The relationship between young stellar clusters and respective parental molecular clouds is still an open issue: for instance, are the similarities between substructures of clouds and clusters just a coincidence? Or would they be the indication of a physical relationship? In order to address these issues, we have studied the CMa OB1/R1 region that shows evidence for a complex star formation history. We obtained molecular clouds mapping with the IRAM-30 metre telescope to reveal the physical conditions of an unexplored side of the CMa region aiming to compare the morphology of the clouds with the distribution of the young stellar objects (YSOs). We also study the clouds kinematics searching for gradients and jet signatures that could trace different star formation scenarios. The YSOs were selected on the basis of astrometric data from Gaia EDR3 that characterise the moving groups. The distance of $1099^{+25}_{-24}$ pc was obtained for the sample, based on the mean error-weighted parallax. Optical

and near-infrared photometry is used to verify the evolutionary status and circumstellar characteristics of the YSOs. Among the selected candidates we found 40 members associated with the cloud: 1 Class I, 11 Class II, and 28 Class III objects. Comparing the spatial distribution of the stellar population with the cores revealed by the 13CO map, we verify that peaks of emission coincide with the position of YSOs confirming the association of these objects to their dense natal gas. Our observations support the large-scale scenario of the CMa shell-like structure formed as a relic of successive supernova events.

## 12. Detection of Substructures in Young Transition Disk WL 17

**Hannah Gulick, Sarah Sadavoy, Luca Matra, Patrick Sheehan, Nienke van der Marel** ★ WL 17 is a young transition disk in the Ophiuchus L1688 molecular cloud complex. Even though WL 17 is among the brightest disks in L1688 and massive enough to expect dust self-scattering, it was undetected in polarization down to ALMA's instrument sensitivity limit. Such low polarization fractions could indicate unresolved polarization within the beam or optically thin dust emission. We test the latter case by combining the high sensitivity 233 GHz Stokes I data from the polarization observations with previous ALMA data at 345 GHz and 100 GHz. We use simple geometric shapes to fit the observed disk visibilities in each band. Using our simple models and assumed dust temperature profiles, we estimate the optical depth in all three bands. The optical depth at 233 GHz peaks at $\tau_{233} \sim 0.3$, which suggests the dust emission may not be optically thick enough for dust self-scattering to be efficient. We also find the higher sensitivity 233 GHz data show substructure in the disk for the first time. The substructure appears as brighter lobes along the major axis, on either side of the star. We attempt to fit the lobes with a simple geometric model, but they are unresolved in the 233 GHz data. We propose that the disk may be flared at 1 mm such that there is a higher column of dust along the major axis than the minor axis when viewed at an inclination. These observations highlight the strength of high sensitivity continuum data from dust polarization observations to study disk structures.

## 13. A wide-field CO survey towards the California Molecular Filament

**Weihua Guo, Xuepeng Chen, Jiancheng Feng, Li Sun, Chen Wang, Yang Su, Yan Sun, Yiping Ao, Shaobo Zhang, Xin Zhou, Lixia Yuan, Ji Yang** ★ We present the survey of $^{12}$CO/$^{13}$CO/C$^{18}$O (J=1-0) toward the California Molecular Cloud (CMC) within the region of 161.75° $\leqslant l \leqslant$ 167.75°,-9.5° $\leqslant b \leqslant$-7.5°, using the Purple Mountain Observatory (PMO) 13.7 m millimeter telescope. Adopting a distance of 470 pc, the mass of the observed molecular cloud estimated from $^{12}$CO, $^{13}$CO, and C$^{18}$O is about 2.59×10$^4$ M$_\odot$, 0.85×10$^4$ M$_\odot$, and 0.09×10$^4$ M$_\odot$, respectively. A large-scale continuous filament extending about 72 pc is revealed from the $^{13}$CO images. A systematic velocity gradient perpendicular to the major axis appears and is measured to be $\sim$ 0.82 km s$^{-1}$ pc$^{-1}$. The kinematics along the filament shows an oscillation pattern with a fragmentation wavelength of $\sim$ 2.3 pc and velocity amplitude of $\sim$ 0.92 km s$^{-1}$, which may be related with core-forming flows. Furthermore, assuming an inclination angle to the plane of the sky of 45°, the estimated average accretion rate is $\sim$ 101 M$_\odot$ Myr$^{-1}$ for the cluster LkH$\alpha$ 101 and $\sim$ 21 M$_\odot$ Myr$^{-1}$ for the other regions. In the C$^{18}$O observations, the large-scale filament could be resolved into multiple substructures and their dynamics are consistent with the scenario of filament formation from converging flows. Approximately 225 C$^{18}$O cores are extracted, of which 181 are starless cores. Roughly 37% (67/181) of the starless cores have $\alpha_{\rm vir}$ less than 1. Twenty outflow candidates are identified along the filament. Our results indicate active early-phase star formation along the large-scale filament in the CMC region.

## 14. Which Molecular Cloud Structures Are Bound?

**Neal J. Evans II, Mark Heyer. Marc-Antoine Miville-Deschênes, Quang Nguyen-Luong. Manuel Merello** ★ We analyze surveys of molecular cloud structures defined by tracers ranging from CO $J = 1 - 0$ through $^{13}$CO $J = 1 - 0$ to dust emission together with $NH_3$ data. The mean value of the virial parameter and the fraction of mass in bound structures depends on the method used to identify structures. Generally, the virial parameter decreases and the fraction of mass in bound structures increases with the effective density of the tracer, the surface density and mass of the structures, and the distance from the center of a galaxy. For the most complete surveys of structures in the Galaxy defined by CO $J = 1 - 0$, the fraction of mass that is in bound structures is 0.19. For catalogs of other galaxies based on CO $J = 2 - 1$, the fraction is 0.35. These results offer substantial alleviation of the fundamental problem of slow star formation. If only clouds found to be bound are counted and they are assumed to collapse in a free-fall time at their mean cloud density, the sum over all clouds in a complete survey of the Galaxy yields a predicted star formation rate of 46 solar masses per year, a factor of 6.5 less than if all clouds are bound.

## 15. Touching the Stars: Using High-Resolution 3D Printing to Visualize Stellar Nurseries

**Nia Imara, John C. Forbes, James C. Weaver** ★ Owing to their intricate variable density architecture, and as a principal site of star formation, molecular clouds represent one of the most functionally significant, yet least understood features of our universe. To unravel the intrinsic structural complexity of molecular clouds, here we leverage the power of high-resolution bitmap-based 3D printing, which provides the opportunity to visualize astrophysical structures in a way that uniquely taps into the human brain's ability to recognize patterns suppressed in 2D representations. Using a new suite of nine simulations, each representing different physical extremes in the turbulent interstellar medium, as our source data, our workflow permits the unambiguous visualization of features in the 3D-printed models, such as quasi-planar structures, that are frequently obscured in traditional renderings and animations. Our bitmap-based 3D printing approach thus faithfully reproduces the subtle density gradient distribution within molecular clouds in a tangible, intuitive, and visually stunning manner. While laying the groundwork for the intuitive analysis of other structurally complex astronomical data sets, our 3D-printed models also serve as valuable tools in educational and public outreach endeavors.

## 16. Modeling of CO ro-vibrational line emission of HD 141569

**Stanley K. Jensen Jr., Sean D. Brittain, Joan R. Najita, John S. Carr** ★ HD 141569 is a Herbig Ae/Be star that straddles the boundary between the transition disks and debris disks. It is a low dust mass disk that reveals numerous structural elements (e.g. gaps and rings) that may point to young planets. It also exhibits a reservoir of CO gas observed at both millimeter and IR wavelengths. Previous observations (Goto et al. 2006) reported a possible asymmetry in the CO gas emission. Herein the IR ro-vibrational emission lines are analyzed and modeled both spectroscopically and spectroastrometrically. We find emission features from both 12CO and 13CO isotopologues heated to a temperature of approximately 200 K in the radial extent of 13 to 60 au. We do not see evidenceof the previously reported asymmetry in CO emission, our results being consistent with a Keplerian, axisymmetric emitting region. This raises the question of whether the emission profile may be evolving in time, possibly as a result of an orbiting feature in the inner disk such as a planet.

## 17. Linking Outer Disk Pebble Dynamics and Gaps to Inner Disk Water Enrichment

**A. Kalyaan, P. Pinilla, S. Krijt, G. D. Mulders, A. Banzatti** ★ Millimeter continuum imaging of protoplanetary disks reveals the distribution of solid particles and the presence of substructures (gaps and rings) beyond 5-10 au, while infrared (IR) spectra provide access to abundances of gaseous species at smaller disk radii. Building on recent observational findings of an anti-correlation between the inner disk water luminosity and outer dust disk radius, we aim here at investigating the dynamics of icy solids that drift from the outer disk and sublimate their ice inside the snow line, enriching the water vapor that is observed in the IR. We use a volatile-inclusive disk evolution model to explore a range of conditions (gap location, particle size, disk mass, and alpha-viscosity) under which gaps in the outer disk efficiently block the inward drift of icy solids. We find that inner-disk vapor enrichment is highly sensitive to the location of a disk gap, yielding for each particle size a radial "sweet spot" that reduces the inner-disk vapor enrichment to a minimum. For pebbles of 1-10 mm in size, which carry the most mass, this sweet spot is at 7-15 au, suggesting that inner gaps may have a key role in reducing ice delivery to the inner disk and may not allow the formation of Earths and super-Earths. This highlights the importance of observationally determining the presence and properties of inner gaps in disks. Finally, we argue that the inner water vapor abundance can be used as a proxy for estimating the pebble drift efficiency and mass-flux entering the inner disk.

## 18. Massive young stellar objects in the Local Group irregular galaxy NGC6822 identified using machine learning

**David A. Kinson, Joana M. Oliveira, Jacco Th. van Loon** ★ We present a supervised machine learning methodology to classify stellar populations in the Local Group dwarf-irregular galaxy NGC6822. Near-IR colours (J-H, H-K, and J-K), K-band magnitudes and far-IR surface brightness (at 70 and 160 micron) measured from Spitzer and Herschel images are the features used to train a Probabilistic Random Forest (PRF) classifier. Point-sources are classified into eight target classes: young stellar objects (YSOs), oxygen- and carbon-rich asymptotic giant branch stars, red giant branch and red super-giant stars, active galactic nuclei, massive main-sequence stars and Galactic foreground stars. The PRF identifies sources with an accuracy of 90 percent across all target classes rising to 96 percent for YSOs. We confirm the nature of 125 out of 277 literature YSO candidates with sufficient feature information, and identify

199 new YSOs and candidates. Whilst these are mostly located in known star forming regions, we have also identified new star formation sites. These YSOs have mass estimates between 15-50 Msun, representing the most massive YSO population in NGC 6822. Another 82 out of 277 literature candidates are definitively classified as non-YSOs by the PRF analysis. We characterise the star formation environment by comparing the spatial distribution of YSOs to those of gas and dust using archival images. We also explore the potential of using (unsupervised) t-distributed stochastic neighbour embedding maps for the identification of the same stellar population classified by the PRF.

## 19. The Near Stellar Environment of Class 0 Protostars: A First Look with Near-Infrared Spectroscopy

**S. Laos, T. P. Greene, J. R. Najita, K. G. Stassun** ★ We present near-infrared K-band spectra for a sample of 7 Class 0 protostars in the Perseus and Orion star-forming regions. We detect Br gamma, CO overtone, and H2 emission, features that probe the near circumstellar environment of the protostar and reveal evidence of magnetospheric accretion, a hot inner disk atmosphere, and outflows, respectively. Comparing the properties of these features with those of Class I sources from the literature, we find that their Br gamma and CO emission are generally consistent in strength and velocity width. The Br gamma line profiles are broad and centrally peaked, with FWHMs of 200 km/s and wings extending to 300 km/s. The line ratios of our H2 emission features, which are spatially extended for some sources, are consistent with shock excitation and indicate the presence of strong jets or a disk wind. Within our small sample, the frequency of CO band emission (67%) is high relative to that of Class I samples (15%), indicating that Class 0s have high inner disk accretion rates, similar to those of the most actively accreting Class I sources. Collectively, our results suggest that Class 0 sources have similar accretion mechanisms to the more evolved classes, with strong organized stellar magnetic fields established at the earliest observable stage of evolution.

## 20. Molecules with ALMA at Planet-forming Scales (MAPS) III: Characteristics of Radial Chemical Substructures

**Charles J. Law, Ryan A. Loomis, Richard Teague, Karin I. Öberg, Ian Czekala, Sean M. Andrews, Jane Huang, Yuri Aikawa, Felipe Alarcón, Jaehan Bae, Edwin A. Bergin, Jennifer B. Bergner, Yann Boehler, Alice S. Booth, Arthur D. Bosman, Jenny K. Calahan, Gianni Cataldi, L. Ilsedore Cleeves, Kenji Furuya, Viviana V. Guzmán, John D. Ilee, Romane Le Gal, Yao Liu, Feng Long, François Ménard, Hideko Nomura, Chunhua Qi, Kamber R. Schwarz, Anibal Sierra, Takashi Tsukagoshi, Yoshihide Yamato, Merel L. R. van't Hoff, Catherine Walsh, David J. Wilner, Ke Zhang** ★ The Molecules with ALMA at Planet-forming Scales (MAPS) Large Program provides a detailed, high resolution (∼10-20 au) view of molecular line emission in five protoplanetary disks at spatial scales relevant for planet formation. Here, we present a systematic analysis of chemical substructures in 18 molecular lines toward the MAPS sources: IM Lup, GM Aur, AS 209, HD 163296, and MWC 480. We identify more than 200 chemical substructures, which are found at nearly all radii where line emission is detected. A wide diversity of radial morphologies - including rings, gaps, and plateaus - is observed both within each disk and across the MAPS sample. This diversity in line emission profiles is also present in the innermost 50 au. Overall, this suggests that planets form in varied chemical environments both across disks and at different radii within the same disk. Interior to 150 au, the majority of chemical substructures across the MAPS disks are spatially coincident with substructures in the millimeter continuum, indicative of physical and chemical links between the disk midplane and warm, elevated molecular emission layers. Some chemical substructures in the inner disk and most chemical substructures exterior to 150 au cannot be directly linked to dust substructure, however, which indicates that there are also other causes of chemical substructures, such as snowlines, gradients in UV photon fluxes, ionization, and radially-varying elemental ratios. This implies that chemical substructures could be developed into powerful probes of different disk characteristics, in addition to influencing the environments within which planets assemble. This paper is part of the MAPS special issue of the Astrophysical Journal Supplement.

## 21. Molecules with ALMA at Planet-forming Scales (MAPS) IV: Emission Surfaces and Vertical Distribution of Molecules

**Charles J. Law, Richard Teague, Ryan A. Loomis, Jaehan Bae, Karin I. Öberg, Ian Czekala, Sean M. Andrews, Yuri Aikawa, Felipe Alarcón, Edwin A. Bergin, Jennifer B. Bergner, Alice S. Booth, Arthur D. Bosman, Jenny K. Calahan, Gianni Cataldi, L. Ilsedore Cleeves, Kenji Furuya, Viviana V. Guzmán, Jane Huang, John D. Ilee, Romane Le Gal, Yao Liu, Feng Long, François Ménard, Hideko Nomura, Laura M. Pérez, Chunhua Qi, Kamber**

**R. Schwarz, Daniela Soto, Takashi Tsukagoshi, Yoshihide Yamato, Merel L. R. van't Hoff, Catherine Walsh, David J. Wilner, Ke Zhang** ★ The Molecules with ALMA at Planet-forming Scales (MAPS) Large Program provides a unique opportunity to study the vertical distribution of gas, chemistry, and temperature in the protoplanetary disks around IM Lup, GM Aur, AS 209, HD 163296, and MWC 480. By using the asymmetry of molecular line emission relative to the disk major axis, we infer the emission height ($z$) above the midplane as a function of radius ($r$). Using this method, we measure emitting surfaces for a suite of CO isotopologues, HCN, and $C_2H$. We find that $^{12}CO$ emission traces the most elevated regions with $z/r > 0.3$, while emission from the less abundant $^{13}CO$ and $C^{18}O$ probes deeper into the disk at altitudes of $z/r \lesssim 0.2$. $C_2H$ and HCN have lower opacities and SNRs, making surface fitting more difficult, and could only be reliably constrained in AS 209, HD 163296, and MWC 480, with $z/r \lesssim 0.1$, i.e., relatively close to the planet-forming midplanes. We determine peak brightness temperatures of the optically thick CO isotopologues and use these to trace 2D disk temperature structures. Several CO temperature profiles and emission surfaces show dips in temperature or vertical height, some of which are associated with gaps and rings in line and/or continuum emission. These substructures may be due to local changes in CO column density, gas surface density, or gas temperatures, and detailed thermo-chemical models are necessary to better constrain their origins and relate the chemical compositions of elevated disk layers with those of planet-forming material in disk midplanes. This paper is part of the MAPS special issue of the Astrophysical Journal Supplement.

## 22. The JCMT Transient Survey: Four Year Summary of Monitoring the Submillimeter Variability of Protostars

**The JCMT Transient Survey Collaboration - Yong-Hee Lee et al.** ★ We present the four-year survey results of monthly submillimeter monitoring of eight nearby (< 500pc) star-forming regions by the JCMT Transient Survey. We apply the Lomb-Scargle Periodogram technique to search for and characterize variability on 295 submillimeter peaks brighter than 0.14 Jy beam$^{-1}$, including 22 disk sources (Class II), 83 protostars (Class 0/I), and 190 starless sources. We uncover 18 secular variables, all of them protostars. No single-epoch burst or drop events and no inherently stochastic sources are observed. We classify the secular variables by their timescales into three groups: Periodic, Curved, and Linear. For the Curved and Periodic cases, the detectable fractional amplitude, with respect to mean peak brightness, is $\sim 4$ % for sources brighter than $\sim 0.5$ Jy beam$^{-1}$. Limiting our sample to only these bright sources, the observed variable fraction is 37% (16 out of 43). Considering source evolution, we find a similar fraction of bright variables for both Class 0 and Class I. Using an empirically motivated conversion from submillimeter variability to variation in mass accretion rate, six sources (7% of our full sample) are predicted to have years-long accretion events during which the excess mass accreted reaches more than 40% above the total quiescently accreted mass: two previously known eruptive Class I sources, V1647 Ori and EC 53 (V371 Ser), and four Class 0 sources, HOPS 356, HOPS 373, HOPS 383, and West 40. Considering the full protostellar ensemble, the importance of episodic accretion on few years timescale is negligible, only a few percent of the assembled mass. However, given that this accretion is dominated by events of order the observing time-window, it remains uncertain as to whether the importance of episodic events will continue to rise with decades-long monitoring.

## 23. The discovery of the largest gas filament in our Galaxy, or a new spiral arm?

**Chong Li, Keping Qiu, Bo Hu, Yue Cao** ★ Using the Five-hundred-meter Aperture Spherical radio Telescope (FAST), we detect a giant HI filamentary structure in the sky region of $307.^\circ7 < \alpha < 311.^\circ0$ and $40.^\circ9 < \delta < 43.^\circ4$. The structure has a velocity range of $-170$ km s$^{-1}$ to $-130$ km s$^{-1}$, and a mean velocity of $-150$ km s$^{-1}$, putting it to a Galactocentric distance of 22 kpc. The HI structure has a length of 1.1 kpc, which appears to be so far the furthest and largest giant filament in the Galaxy and we name it Cattail. Its mass is calculated to be $6.5 \times 10^4$ M$_\odot$ and the linear mass density is 60 M$_\odot$ pc$^{-1}$. Its width is 207 pc, corresponding to an aspect ratio of 5:1. Cattail possesses a small velocity gradient (0.02 km s$^{-1}$ pc$^{-1}$) along its major axis. Together with the HI4PI data, we find that Cattail could have an even larger length, up to 5 kpc. We also identify another new elongated structure to be the extension into the Galactic first quadrant of the Outer Scutum-Centaurus (OSC) arm, and Cattail appears to be located far behind the OSC. The question about how such a huge filament is produced at the extreme Galactic location remains open. Alternatively, Cattail might be part of a new arm beyond the OSC, though it is puzzling that the structure does not fully follow the warp of the Galactic disk.

## 24. Physical Properties and Real Nature of Massive Clumps in the Galaxy

**Zu-Jia Lu, Veli-Matti Pelkonen, Mika Juvela, Paolo Padoan, Troels Haugbølle, Åke Nordlund** ★ Systematic surveys of massive clumps have been carried out to study the conditions leading to the formation of massive stars. These clumps are typically at large distances and unresolved, so their physical properties cannot be reliably derived from the observations alone. Numerical simulations are needed to interpret the observations. To this end, we generate synthetic Herschel observations using our large-scale star-formation simulation, where massive stars explode as supernovae driving the interstellar-medium turbulence. From the synthetic observations, we compile a catalog of compact sources following the exact same procedure as for the Hi-GAL compact source catalog. We show that the sources from the simulation have observational properties with statistical distributions consistent with the observations. By relating the compact sources from the synthetic observations to their three-dimensional counterparts in the simulation, we find that the synthetic observations overestimate the clump masses by about an order of magnitude on average due to line-of-sight projection, and projection effects are likely to be even worse for Hi-GAL Inner Galaxy sources. We also find that a large fraction of sources classified as protostellar are likely to be starless, and propose a new method to partially discriminate between true and false protostellar sources.

## 25. Discovery of a Highly Collimated Flow from the High-Mass Protostar ISOSS J23053+5953 SMM2

**T. M., Rodríguez, P. Hofner, E. D. Araya, Q. Zhang, H. Linz, S. Kurtz, L. Gómez, C. Carrasco-González, V. Rosero** ★ We present Very Large Array C, X, and Q-band continuum observations, as well as 1.3 mm continuum and CO(2-1) observations with the Submillimeter Array toward the high-mass protostellar candidate ISOSS J23053+5953 SMM2. Compact cm continuum emission was detected near the center of the SMM2 core with a spectral index of 0.24 between 6 and 3.6 cm, and a radio luminosity of 1.3 mJy kpc$^2$. The 1.3 mm thermal dust emission indicates a mass of the SMM2 core of 45.8 Msun. The CO(2-1) observations reveal a large, massive molecular outflow centered on the SMM2 core. This fast outflow ($>$ 50 km/s from the cloud systemic velocity) is highly collimated, with a broader, lower-velocity component. The large values for outflow mass (45.2 Msun), and momentum rate (6 x $10^{-3}$ Msun km/s/yr) derived from the CO emission are consistent with those of flows driven by high-mass YSOs. The dynamical timescale of the flow is between 1.5 - 7.2 x $10^4$ yr. We also found from the C18O to thermal dust emission ratio that CO is depleted by a factor of about 20, possibly due to freeze out of CO molecules on dust grains. Our data are consistent with previous findings that ISOSS J23053+5953 SMM2 is an emerging high-mass protostar in an early phase of evolution, with an ionized jet, and a fast, highly collimated, and massive outflow.

## 26. Dynamical effects of the radiative stellar feedback on the H I-to-H2 transition

**Vincent Maillard, Emeric Bron, Franck Le Petit** ★ The atomic-to-molecular hydrogen (H/H2) transition has been extensively studied as it controls the fraction of gas in a molecular state in an interstellar cloud. This fraction is linked to star-formation by the Schmidt-Kennicutt law. While theoretical estimates of the column density of the H I layer have been proposed for static photodissociation regions (PDRs), Herschel and well-resolved ALMA (Atacama Large Millimeter Array) observations have revealed dynamical effects in star forming regions, caused by the process of photoevaporation. We extend the analytic study of the H/H2 transition to include the effects of the propagation of the ionization front, in particular in the presence of photoevaporation at the walls of blister H II regions, and we find its consequences on the total atomic hydrogen column density at the surface of clouds in the presence of an ultraviolet field, and on the properties of the H/H2 transition. We solved semi-analytically the differential equation giving the H2 column density profile by taking into account H2 formation on grains, H2 photodissociation, and the ionization front propagation dynamics modeled as advection of the gas through the ionization front. Taking this advection into account reduces the width of the atomic region compared to static models. The atomic region may disappear if the ionization front velocity exceeds a certain value, leading the H/H2 transition and the ionization front to merge. For both dissociated and merged configurations, we provide analytical expressions to determine the total H I column density. Our results take the metallicity into account. Finally, we compared our results to observations of PDRs illuminated by O-stars, for which we conclude that the dynamical effects are strong, especially for low-excitation PDRs.

## 27. Characterization of the dust content in the ring around Sz 91: indications for planetesimal formation?

**Karina Maucó, Carlos Carrasco-González, Matthias R. Schreiber, Anibal Sierra, Johan Olofsson, Amelia Bayo, Claudio Caceres, Hector Canovas, Aina Palau** ★ One of the most important questions in the field of planet formation is how mm-cm sized dust particles overcome the radial drift and fragmentation barriers to form kilometer-sized planetesimals. ALMA observations of protoplanetary disks, in particular transition disks or disks with clear signs of substructures, can provide new constraints on theories of grain growth and planetesimal formation and therefore represent one possibility to progress on this issue. We here present ALMA band 4 (2.1 mm) observations of the transition disk system Sz 91 and combine them with previously obtained band 6 (1.3 mm) and 7 (0.9 mm) observations. Sz 91 with its well defined mm-ring, more extended gas disk, and evidence of smaller dust particles close to the star, is a clear case of dust filtering and the accumulation of mm sized particles in a gas pressure bump. We computed the spectral index (nearly constant at ∼3.34), optical depth (marginally optically thick), and maximum grain size (∼ 0.61 mm) in the dust ring from the multi-wavelength ALMA observations and compared the results with recently published simulations of grain growth in disk substructures. Our observational results are in very good agreement with the predictions of models for grain growth in dust rings that include fragmentation and planetesimal formation through the streaming instability.

## 28. Signatures of UV radiation in low-mass protostars I. Origin of HCN and CN emission in the Serpens Main region

**A. Mirocha, A. Karska, M. Gronowski, L. E. Kristensen, Ł. Tychoniec, D. Harsono, M. Figueira, M. Gładkowski, M. Żółtowski** ★ Context: Ultraviolet radiation (UV) influences the physics and chemistry of star-forming regions, but its properties and significance in the immediate surroundings of low-mass protostars are still poorly understood. Aims: We aim to extend the use of the CN/HCN ratio, already established for high-mass protostars, to the low-mass regime to trace and characterize the UV field around low-mass protostars on $\sim 0.6 \times 0.6$ pc scales. Methods: We present $5' \times 5'$ maps of the Serpens Main Cloud encompassing 10 protostars observed with the EMIR receiver at the IRAM 30 m telescope in CN 1-0, HCN 1-0, CS 3-2, and some of their isotopologues. The radiative-transfer code RADEX and the chemical model Nahoon are used to determine column densities of molecules, gas temperature and density, and the UV field strength, $G_0$. Results: The spatial distribution of HCN and CS are well-correlated with CO 6-5 emission that traces outflows. The CN emission is extended from the central protostars to their immediate surroundings also tracing outflows, likely as a product of HCN photodissociation. The ratio of CN to HCN total column densities ranges from ∼1 to 12 corresponding to $G_0 \approx 10^1 - 10^3$ for gas densities and temperatures typical for outflows of low-mass protostars. Conclusions: UV radiation associated with protostars and their outflows is indirectly identified in a significant part of the Serpens Main low-mass star-forming region. Its strength is consistent with the values obtained from the OH and $H_2O$ ratios observed with Herschel and compared with models of UV-illuminated shocks. From a chemical viewpoint, the CN to HCN ratio is an excellent tracer of UV fields around low- and intermediate-mass star-forming regions.

## 29. The ALMA Survey of 70 $\mu$m Dark High-mass Clumps in Early Stages (ASHES). IV. Star formation signatures in G023.477

**Kaho Morii, Patricio Sanhueza, Fumitaka Nakamura, James M. Jackson, Shanghuo Li, Henrik Beuther, Qizhou Zhang, Siyi Feng, Daniel Tafoya, Andrés E. Guzmán, Natsuko Izumi, Takeshi Sakai, Xing Lu, Ken'ichi Tatematsu, Satoshi Ohashi, Andrea Silva, Fernando A. Olguin, Yanett Contreras** ★ With a mass of ∼1000 $M_\odot$ and a surface density of ∼0.5 g cm$^{-2}$, G023.477+0.114 also known as IRDC 18310-4 is an infrared dark cloud (IRDC) that has the potential to form high-mass stars and has been recognized as a promising prestellar clump candidate. To characterize the early stages of high-mass star formation, we have observed G023.477+0.114 as part of the ALMA Survey of 70 $\mu$m Dark High-mass Clumps in Early Stages (ASHES). We have conducted ∼1."2 resolution observations with the Atacama Large Millimeter/submillimeter Array (ALMA) at 1.3 mm in dust continuum and molecular line emission. We identified 11 cores, whose masses range from 1.1 $M_\odot$ to 19.0 $M_\odot$. Ignoring magnetic fields, the virial parameters of the cores are below unity, implying that the cores are gravitationally bound. However, when magnetic fields are included, the prestellar cores are close to virial equilibrium, while the protostellar cores remain sub-virialized. Star formation activity has already started in this clump. Four collimated outflows are detected in CO and SiO. $H_2CO$ and $CH_3OH$ emission coincide with the high-velocity components seen in the CO and SiO emission. The outflows are randomly oriented for the natal filament and the magnetic field. The position-velocity diagrams suggest that episodic mass ejection has already begun even in this very early phase of protostellar formation. The masses of the identified

cores are comparable to the expected maximum stellar mass that this IRDC could form (8-19 $M_{\odot}$). We explore two possibilities on how IRDC G023.477+0.114 could eventually form high-mass stars in the context of theoretical scenarios.

## 30. Interpretation of optical and IR light curves for transitional disk candidates in NGC 2264 using the extincted stellar radiation and the emission of optically thin dust inside the hole

**Erick Nagel, Fernando Gutiérrez-Canales, Sebastián Morales-Gutiérrez, Alana P. Sousa** ★ In the stellar forming region NGC 2264 there are objects catalogued as hosting a transitional disk according to spectrum modeling. Four members of this set have optical and infrared light curves coming from the CoRoT and Spitzer telescopes. In this work, we try to simultaneously explain the light curves using the extinction of the stellar radiation and the emission of the dust inside the hole of a transitional disk. For the object Mon-296, we were successful. However, for Mon-314, and Mon-433 our evidence suggests that they host a pre-transitional disk. For Mon-1308 a new spectrum fitting using the 3D radiative transfer code Hyperion allows us to conclude that this object hosts a full disk instead of a transitional disk. This is in accord to previous work on Mon-1308 and with the fact that we cannot find a fit for the light curves using only the contribution of the dust inside the hole of a transitional disk.

## 31. Quantifying Variability of YSOs in the Mid-IR Over Six Years with NEOWISE

**Wooseok Park, Jeong-Eun Lee, Carlos Contreras Peña, Doug Johnstone, Gregory Herczeg, Sieun Lee, Seonjae Lee, Anupam Bhardwaj, Gerald H. Moriarty-Schieven** ★ Variability in young stellar objects (YSOs) can be caused by various time-dependent phenomena associated with star formation, including accretion rates, geometric changes in the circumstellar disks, stochastic hydromagnetic interactions between stellar surfaces and inner disk edges, reconnections within the stellar magnetosphere, and hot/cold spots on stellar surfaces. We uncover and characterize ∼1700 variables from a sample of ∼5400 YSOs in nearby low-mass star-forming regions using mid-IR light curves obtained from the 6.5-years NEOWISE All Sky Survey. The mid-IR variability traces a wide range of dynamical, physical, and geometrical phenomenon. We classify six types of YSO mid-IR variability based on their light curves: secular variability ($Linear, Curved, Periodic$) and stochastic variability ($Burst, Drop, Irregular$). YSOs in earlier evolutionary stages have higher fractions of variables and higher amplitudes for the variability, with the recurrence timescale of FUor-type outbursts (defined here as $\Delta$W1 or $\Delta$W2 $> 1$ mag followed by inspection of candidates) of ∼1000 years in the early embedded protostellar phase. Known eruptive young stars and subluminous objects show fractions of variables similar to the fraction ($\sim 55\%$) found in typical protostars, suggesting that these two distinct types are not distinct in variability over the 6.5-year timescale. Along with brightness variability, we also find a diverse range of secular color variations, which can be attributed to a competitive interplay between the variable accretion luminosity of the central source and the variable extinction by material associated with the accretion process.

## 32. The first spectroscopically confirmed brown dwarfs in NGC 2264

**Samuel Pearson, Aleks Scholz, Paula S Teixeira, Koraljka Mužić, Víctor Almendros-Abad** ★ We present spectroscopic follow-up observations of 68 red, faint candidates from our multi-epoch, multi-wavelength, previously published survey of NGC 2264. Using near-infrared spectra from VLT/KMOS, we measure spectral types and extinction for 32 young low-mass sources. We confirm 13 as brown dwarfs in NGC 2264, with spectral types between M6 and M8, corresponding to masses between 0.02 and $0.08 M_{\odot}$. These are the first spectroscopically confirmed brown dwarfs in this benchmark cluster. 19 more objects are found to be young M-type stars of NGC 2264 with masses of 0.08 to $0.3\,M_{\odot}$. 7 of the confirmed brown dwarfs as well as 15 of the M-stars have IR excess caused by a disc. Comparing with isochrones, the typical age of the confirmed brown dwarfs is <0.5 to 5Myr. More than half of the newly identified brown dwarfs and very low mass stars have ages <0.5Myr, significantly younger than the bulk of the known cluster population. Based on the success rate of our spectroscopic follow-up, we estimate that NGC 2264 hosts 200-600 brown dwarfs in total (in the given mass range). This would correspond to a star-to-brown dwarf ratio between 2.5:1 and 7.5:1. We determine the slope of the substellar mass function as $\alpha = 0.43^{+0.41}_{-0.56}$, these values are consistent with those measured for other young clusters. This points to a uniform substellar mass function across all star forming environments.

## 33. Close stellar flybys common in low-mass clusters

**Susanne Pfalzner, Amith Govind** ★ Numerous protoplanetary discs show distinct spiral arms features. While possibly caused by a range of processes, detailed pattern analysis points at close stellar flybys as cause for some of them. Surprisingly, these discs reside in young low-mass clusters, where close stellar flybys are expected to be rare. This fact motivated us to take a fresh look at the frequency of close flybys in low-mass clusters. In the solar neighbourhood, low-mass clusters have smaller half-mass radii than their more massive counterparts. We show that this observational fact results in the mean and central stellar density of low-mass clusters being approximately the same as in high-mass clusters, which is rarely reflected in theoretical studies. We perform N-body simulations of the stellar dynamics in young clusters obeying the observed mass-radius relation. Taking the mean disc truncation radius as a proxy for the degree of influence of the environment, we find that the influence of the environment on discs is more or less the same in low- and high-mass clusters. Even the fraction of small discs($<$ 10 au) is nearly identical. Our main conclusion is that the frequency of close flybys seems to have been severely underestimated for low-mass clusters. A testable prediction of this hypothesis is that low-mass clusters should contain 10%-15% of discs smaller than 30 au truncated by flybys. These truncated discs should be distinguishable from primordially small discs by their steep outer edge.

## 34. An unbiased NOEMA 2.6 to 4 mm survey of the GG Tau ring: First detection of CCS in a protoplanetary disk

**N. T. Phuong, A. Dutrey, E. Chapillon, S. Guilloteau, J. Bary, T. L. Beck, A. Coutens, O. Denis-Alpizar, E. Di Folco, P. N. Diep, L. Majumdar, J-P. Melisse, C-W. Lee, V. Pietu, T. Stoecklin, Y-W. Tang** ★ Molecular line surveys are among the main tools to probe the structure and physical conditions in protoplanetary disks (PPDs), the birthplace of planets. The large radial and vertical temperature as well as density gradients in these PPDs lead to a complex chemical composition, making chemistry an important step to understand the variety of planetary systems. We aimed to study the chemical content of the protoplanetary disk surrounding GG Tau A, a well-known triple T Tauri system. We used NOEMA with the new correlator PolyFix to observe rotational lines at 2.6 to 4 mm from a few dozen molecules. We analysed the data with a radiative transfer code to derive molecular densities and the abundance relative to $^{13}$CO, which we compare to those of the TMC1 cloud and LkCa15 disk. We report the first detection of CCS in PPDs. We also marginally detect OCS and find 16 other molecules in the GG Tauri outer disk. Ten of them had been found previously, while seven others ($^{13}$CN, $N_2H^+$, HNC, DNC, $HC_3N$, CCS, and C$^{34}$S) are new detections in this disk. The analysis confirms that sulphur chemistry is not yet properly understood. The D/H ratio, derived from $DCO^+/HCO^+$, DCN/HCN, and DNC/HNC ratios, points towards a low temperature chemistry. The detection of the rare species CCS confirms that GG Tau is a good laboratory to study the protoplanetary disk chemistry, thanks to its large disk size and mass.

## 35. An orbital release model for the Orion BN/KL fingers

**A. C. Raga, P. R. Rivera-Ortiz, A. Rodriguez-Gonzalez, A. Castellanos-Ramirez** ★ We present a simple model in which the bullets that produce the "Orion fingers" (ejected by the BN/KL object) are interpreted as protoplanets or low mass protostars in orbit around a high mass star that has a supernova explosion. As the remnant of the SN explosion has only a small fraction of the mass of the pre-supernova star, the orbiting objects then move away in free trajectories, preserving their orbital velocity at the time of release. We show that a system of objects arranged in approximately co-planar orbits results in trajectories with morphological and kinematical characteristics resembling the Orion fingers. We show that, under the assumption of constant velocity motions, the positions of the observed heads of the fingers can be used to reconstruct the properties of the orbital structure from which they originated, resulting in a compact disk with an outer radius of $\sim 2.4$ AU.

## 36. Globules and pillars in Cygnus X III. Herschel and upGREAT/SOFIA far-infrared spectroscopy of the globule IRAS 20319+3958 inCygnus X

**N. Schneider, M. Roellig, E. T. Polehampton, F. Comeron, A. A. Djupvik, Z. Makai, C. Buchbender, R. Simon, S. Bontemps, R. Guesten, G. White, Y. Okada, A. Parikka, N. Rothbart** ★ IRAS 20319+3958 in Cygnus X South is a rare example of a free-floating globule (mass 240 Msun, length 1.5 pc) with an internal HII region created by the stellar feedback of embedded intermediate-mass stars, in particular, one Herbig Be star. Here, we present a Herschel/HIFI CII 158 mu map of the whole globule and a large set of other FIR lines (mid-to high-J CO lines observed with Herschel/PACS and SPIRE, the OI 63 mu line and the CO 16-15 line observed with upGREAT on SOFIA), covering the globule head and partly a position in the tail. The CII map revealed that the whole globule is probably rotating. Highly collimated, high-velocity CII emission is detected close to the Herbig Be star. We performed a PDR analysis using the KOSMA-tau PDR code for one position in the head and one in the tail. The observed FIR lines in the head can be reproduced with a two-component model: an extended, non-clumpy outer PDR shell and a clumpy, dense, and thin inner PDR layer, representing the interface between the HII region cavity and the external PDR. The modelled internal UV field of 2500 Go is similar to what we obtained from the Herschel FIR fluxes, but lower than what we estimated from the census of the embedded stars. External illumination from the 30 pc distant Cyg OB2 cluster, producing an UV field of 150-600 G0 as an upper limit, is responsible for most of the CII emission. For the tail, we modelled the emission with a non-clumpy component, exposed to a UV-field of around 140 Go.

## 37. Are massive dense clumps truly sub-virial? A new analysis using Gould Belt ammonia data

**Ayushi Singh, Christopher D. Matzner, Rachel K. Friesen, Peter G. Martin, Jaime E. Pineda, Erik W. Rosolowsky, Felipe Alves, Ana Chacón-Tanarro, Hope How-Huan Chen, Michael Chun-Yuan Chen, Spandan Choudhury, James Di Francesco, Jared Keown, Helen Kirk, Anna Punanova, Youngmin Seo, Yancy Shirley, Adam Ginsburg, Stella S. R. Offner, Héctor G. Arce, Paola Caselli, Alyssa A. Goodman, Philip C. Myers, Elena Redaelli** ★ Dynamical studies of dense structures within molecular clouds often conclude that the most massive clumps contain too little kinetic energy for virial equilibrium, unless they are magnetized to an unexpected degree. This raises questions about how such a state might arise, and how it might persist long enough to represent the population of massive clumps. In an effort to re-examine the origins of this conclusion, we use ammonia line data from the Green Bank Ammonia Survey and Planck-calibrated dust emission data from Herschel to estimate the masses and kinetic and gravitational energies for dense clumps in the Gould Belt clouds. We show that several types of systematic error can enhance the appearance of low kinetic-to-gravitational energy ratios: insufficient removal of foreground and background material; ignoring the kinetic energy associated with velocity differences across a resolved cloud; and over-correcting for stratification when evaluating the gravitational energy. Using an analysis designed to avoid these errors, we find that the most massive Gould Belt clumps harbor virial motions, rather than sub-virial ones. As a byproduct, we present a catalog of masses, energies, and virial energy ratios for 85 Gould Belt clumps.

## 38. Kinetic temperature of massive star-forming molecular clumps measured with formaldehyde IV. The ALMA view of N113 and N159W in the LMC

**X. D. Tang, C. Henkel, K. M. Menten, Y. Gong, C. -H. R. Chen, D. L. Li, M. -Y. Lee, J. G. Mangum, Y. P. Ao, S. Mühle, S. Aalto, S. García-Burillo, S. Martín, S. Viti, S. Muller, F. Costagliola, H. Asiri, S. A. Levshakov, M. Spaans, J. Ott, C. M. V. Impellizzeri, Y. Fukui, Y. X. He, J. Esimbek, J. J. Zhou, X. W. Zheng, X. Zhao, J. S. Li** ★ We mapped the kinetic temperature structure of two massive star-forming regions, N113 and N159W, in the Large Magellanic Cloud (LMC). We have used $\sim$1.″6 ($\sim$0.4 pc) resolution measurements of the para-$H_2CO$ $J_{K_aK_c} = 3_{03}$–$2_{02}$, $3_{22}$–$2_{21}$, and $3_{21}$–$2_{20}$ transitions near 218.5 GHz to constrain RADEX non-LTE models of the physical conditions. The gas kinetic temperatures derived from the para-$H_2CO$ line ratios $3_{22}$–$2_{21}/3_{03}$–$2_{02}$ and $3_{21}$–$2_{20}/3_{03}$–$2_{02}$ range from 28 to 105 K in N113 and 29 to 68 K in N159W. Distributions of the dense gas traced by para-$H_2CO$ agree with those of the 1.3 mm dust and *Spitzer* 8.0 $\mu$m emission, but do not significantly correlate with the H$\alpha$ emission. The high kinetic temperatures ($T_{\rm kin} \gtrsim 50$ K) of the dense gas traced by para-$H_2CO$ appear to be correlated with the embedded infrared sources inside the clouds and/or YSOs in the N113 and N159W regions. The lower temperatures ($T_{\rm kin} < 50$ K) are measured at the outskirts of the $H_2CO$-bearing distributions of both N113 and N159W. It seems that the kinetic temperatures of the dense gas traced by para-$H_2CO$ are weakly affected by the external sources of the H$\alpha$ emission. The non-thermal velocity dispersions of para-$H_2CO$ are well correlated with the gas kinetic temperatures in the N113 region, implying that the higher kinetic temperature traced by para-$H_2CO$ is

related to turbulence on a ∼0.4 pc scale. The dense gas heating appears to be dominated by internal star formation activity, radiation, and/or turbulence. It seems that the mechanism heating the dense gas of the star-forming regions in the LMC is consistent with that in Galactic massive star-forming regions located in the Galactic plane.

## 39. Chemical compositions in the vicinity of protostars in Ophiuchus

**Kotomi Taniguchi, Liton Majumdar, Adele Plunkett, Shigehisa Takakuwa, Dariusz C. Lis, Paul F. Goldsmith, Fumitaka Nakamura, Masao Saito, Eric Herbst** ★ We have analyzed Atacama Large Millimeter/submillimeter Array (ALMA) Cycle 4 Band 6 data toward two young stellar objects (YSOs), Oph-emb5 and Oph-emb9, in the Ophiuchus star-forming region. The YSO Oph-emb5 is located in a relatively quiescent region, whereas Oph-emb9 is irradiated by a nearby bright Herbig Be star. Molecular lines from *cyclic*-$C_3H_2$ ($c$-$C_3H_2$), $H_2CO$, $CH_3OH$, $^{13}CO$, $C^{18}O$, and $DCO^+$ have been detected from both sources, while DCN is detected only in Oph-emb9. Around Oph-emb5, $c$-$C_3H_2$ is enhanced at the west side, relative to the IR source, whereas $H_2CO$ and $CH_3OH$ are abundant at the east side. In the field of Oph-emb9, moment 0 maps of the $c$-$C_3H_2$ lines show a peak at the eastern edge of the field of view, which is irradiated by the Herbig Be star. Moment 0 maps of $CH_3OH$ and $H_2CO$ show peaks farther from the bright star. We derive the $N(c\text{-}C_3H_2)/N(CH_3OH)$ column density ratios at the peak positions of $c$-$C_3H_2$ and $CH_3OH$ near each YSO, which are identified based on their moment 0 maps. The $N(c\text{-}C_3H_2)/N(CH_3OH)$ ratio at the $c$-$C_3H_2$ peak is significantly higher than at the $CH_3OH$ peak by a factor of $\sim$ 19 in Oph-emb9, while the difference in this column density ratio between these two positions is a factor of $\sim$ 2.6 in Oph-emb5. These differences are attributed to the efficiency of the photon-dominated region (PDR) chemistry in Oph-emb9. The higher $DCO^+$ column density and the detection of DCN in Oph-emb9 are also discussed in the context of UV irradiation flux.

## 40. Clump-scale chemistry in the NGC2264-D cluster-forming region

**Kotomi Taniguchi, Adele Plunkett, Tomomi Shimoikura, Kazuhito Dobashi, Masao Saito, Fumitaka Nakamura, Eric Herbst** ★ We have conducted mapping observations toward the n3 and n5 positions in the NGC 2264-D cluster-forming region with the Atacama Compact Array (ACA) of the Atacama Large Millimeter/submillimeter Array (ALMA) in Band 3. Observations with 10000 au scale beam reveal the chemical composition at the clump scale. The spatial distributions of the observed low upper-state-energy lines of $CH_3OH$ are similar to those of CS and SO, and the $HC_3N$ emission seems to be predominantly associated with clumps containing young stellar objects. The turbulent gas induced by the star formation activities produces large-scale shock regions in NGC 2264-D, which are traced by the $CH_3OH$, CS and SO emissions. We derive the $HC_3N$, $CH_3CN$, and $CH_3CHO$ abundances with respect to $CH_3OH$. Compared to the n5 field, the n3 field is farther (in projected apparent distance) from the neighboring NGC 2264-C, yet the chemical composition in the n3 field tends to be similar to that of the protostellar candidate CMM3 in NGC 2264-C. The $HC_3N/CH_3OH$ ratios in the n3 field are higher than those in the n5 field. We find an anti-correlation between the $HC_3N/CH_3OH$ ratio and their excitation temperatures. The low $HC_3N/CH_3OH$ abundance ratio at the n5 field implies that the n5 field is an environment with more active star formation compared with the n3 field.

## An Unbiased CO Survey Toward the Northern Region of the Small Magellanic Cloud with the Atacama Compact Array. I. Overview: CO Cloud Distributions

**Kazuki Tokuda, Hiroshi Kondo, Takahiro Ohno, Ayu Konishi, Hidetoshi Sano, Kisetsu Tsuge, Sarolta Zahorecz, Nao Goto, Naslim Neelamkodan, Tony Wong, Marta Sewiło, Hajime Fukushima, Tatsuya Takekoshi, Kazuyuki Muraoka, Akiko Kawamura, Kengo Tachihara, Yasuo Fukui, Toshikazu Onishi** ★ We have analyzed the data from a large-scale CO survey toward the northern region of the Small Magellanic Cloud (SMC) obtained with the Atacama Compact Array (ACA) stand-alone mode of ALMA. The primary aim of this study is to comprehensively understand the behavior of CO as an $H_2$ tracer in a low-metallicity environment ($Z \sim 0.2\ Z_\odot$). The total number of mosaic fields is ∼8000, which results in a field coverage of 0.26 degree$^2$ ($\sim 2.9 \times 10^5$ pc$^2$), corresponding to ∼10% area of the galaxy. The sensitive ∼2 pc resolution observations reveal the detailed structure of the molecular clouds previously detected in the single-dish NANTEN survey. We have detected a number of compact CO clouds within lower $H_2$ column density ($\sim 10^{20}$ cm$^{-2}$) regions whose angular scale is similar to the ACA beam size. Most of the clouds in this survey also show peak brightness temperature as low as <1 K, which for optically thick CO emission implies an emission size much smaller than the beam size, leading to beam dilution. The comparison between an available estimation of the total molecular material traced by thermal dust emission and the present CO survey demonstrates that more than ∼90% $H_2$ gas cannot be traced by the low-$J$ CO emission. Our processed data cubes and 2-D images are publicly available.

## 42. Protostellar Interferometric Line Survey of the Cygnus X region (PILS-Cygnus) – First results: observations of CygX-N30

**S. J. van der Walt, L. E. Kristensen, J. K. Jørgensen, H. Calcutt, S. Manigand, M. el Akel, R. T. Garrod, K. Qiu** ★ (Abridged) Complex organic molecules (COMs) are commonly detected in and near star-forming regions. However, the dominant process in the release of these COMs from the icy grains - where they predominately form - to the gas phase is still an open question. We investigate the origin of COM emission in a protostellar source, CygX-N30, through high-angular-resolution interferometric observations over a continuous broad frequency range. We used 32 GHz Submillimeter Array observations with continuous frequency coverage from 329 to 361 GHz at an angular resolution of 1" to do a line survey and obtain a chemical inventory of the source. The line emission was used to determine column densities and excitation temperatures for the COMs. We mapped out the intensity distribution of the different species and identified approximately 400 lines that can be attributed to 29 different molecular species and their isotopologues. We find that the molecular peak emission is along a linear gradient, coinciding with the axis of red- and blueshifted H2CO and CS emission. Chemical differentiation is detected along this gradient, with the O-bearing molecular species peaking towards one component of the system and the N- and S-bearing species peaking towards the other. The inferred column densities and excitation temperatures are compared to other sources where COMs are abundant. The origin of the observed COM emission is probably a combination of the young stellar sources along with accretion of infalling material onto a disc-like structure surrounding a young protostar. The low D/H ratio observed (<0.1%) likely reflects a pre-stellar phase where COMs formed on the ices at warm temperatures ( 30 K), with inefficient deuterium fractionation. The observations and results presented here demonstrate the importance of good frequency coverage and high angular resolution when disentangling the origin of COM emission.

## 43. The impact of massive stars and black holes on the fate of open star clusters and their tidal streams

**Long Wang, Tereza Jerabkova** ★ Context: To investigate how the content of massive OB stars affects the long-term evolution of young open clusters and their tidal streams, and how such an effect influences the constraint of initial conditions by looking at the present-day observations. Aims: OB stars are typically in binaries, have a strong wind mass loss during the first few Myr, and many become black holes. These affect the dynamical evolution of an open star cluster and impact its dissolution in a given Galactic potential. We investigate the correlation between the mass of OB stars and the observational properties of open clusters. Hyades-like star clusters are well represented in the Solar neighborhood and thus allow comparisons with observational data. Methods: We perform a large number of star-by-star numerical $N$-body simulations of Hyades-like star clusters by using the high-performance $N$-body code PETAR combined with GALPY. We also developed the tool to transfer the simulation data to mock observations of Gaia. Results: We find that OB stars and black holes have a major effect on star cluster evolution. Star clusters with the same initial conditions, but a different initial content of OB stars, follow very different evolutionary paths. Thus, the initial total mass and radius of an observed star cluster cannot be unambiguously determined unless the initial content of OB stars is known. We show that the stellar counts in the corresponding tidal tails, that can be identified in the Gaia data, help to resolve this issues. We thus emphasise the importance of exploring not only star-clusters, but also their corresponding tidal tails. These findings are relevant for studies of the formation of massive stars.

## 44. In search of infall motion in molecular clumps III: HCO+ (1-0) and H13CO+ (1-0) mapping observations toward the confirmed infall sources

**Yang Yang, Zhibo Jiang, Zhiwei Chen, Yiping Ao, Shuling Yu** ★ The study of infall motion helps us to understand the initial stages of star formation. In this paper, we use the IRAM 30-m telescope to make mapping observations of 24 infall sources confirmed in previous work. The lines we use to track gas infall motions are HCO+ (1-0) and H13CO+ (1-0). All 24 sources show HCO+ emissions, while 18 sources show H13CO+ emissions. The HCO+ integrated intensity maps of 17 sources show clear clumpy structures; for the H13CO+ line, 15 sources show clumpy structures. We estimated the column density of HCO+ and H13CO+ using the RADEX radiation transfer code, and the obtained [HCO+]/[H2] and [H13CO+]/[HCO+] of these sources are about $10^{-}11$ $10^{-}7$ and $10^{-}3$ 1, respectively. Based on the asymmetry of the line profile of the HCO+, we distinguish these sources: 19 sources show blue asymmetric profiles, and the other sources show red profiles or symmetric peak profiles. For eight sources that have double-peaked blue line profiles and signal-to-noise ratios greater than 10, the RATRAN model is used to fit their $HCO^{+}$ (1-0) lines, and to estimate their infall parameters. The mean Vin of these sources are 0.3 1.3 km/s, and the Min are about $10^{-}3$ $10^{-}4$ Msun/yr , which are consistent with the results of intermediate or massive star formation in previous studies. The

Vin estimated from the Myers model are 0.1  1.6 km/s, and the Min are within 10−3  10−5 Msun/yr. In addition, some identified infall sources show other star-forming activities, such as outflows and maser emissions. Especially for those sources with a double-peaked blue asymmetric profile, most of them have both infall and outflow evidence.

## 45. A Morphological Classification of 18190 Molecular Clouds Identified in $^{12}$CO Data from the MWISP Survey

**Lixia Yuan, Ji Yang, Fujun Du, Xunchuan Liu, Shaobo Zhang, Zehao Lin, Jingfei Sun, Qing-Zeng Yan, Yuehui Ma, Yang Su, Yan Sun, Xin Zhou** ★ We attempt to visually classify the morphologies of 18190 molecular clouds, which are identified in the $^{12}$CO(1-0) spectral line data over $\sim$ 450 deg$^2$ of the second Galactic quadrant from the Milky Way Imaging Scroll Painting project (MWISP). Using the velocity-integrated intensity maps of the $^{12}$CO(1-0) emission, molecular clouds are first divided into unresolved and resolved ones. The resolved clouds are further classified as non-filaments or filaments. Among the 18190 molecular clouds, $\sim$ 25 % are unresolved, $\sim$ 64% are non-filaments, and $\sim$ 11% are filaments. In the terms of the integrated flux of $^{12}$CO(1-0) spectra of the whole 18190 molecular clouds, $\sim$ 90% are from filaments, $\sim$ 9% are from non-filaments, and the rest $\sim$ 1% are from unresolved sources. Although non-filaments are dominant in the number of the discrete molecular clouds, filaments are the main contributor of $^{12}$CO emission flux. We also present the number distributions of physical parameters of the molecular clouds in our catalog, including their angular sizes, velocity spans, peak intensities of $^{12}$CO(1-0) emission, and $^{12}$CO(1-0) total fluxes. We find that there is a systematic difference between the angular sizes of the non-filaments and filaments, with the filaments tending to have larger angular scales. The $H_2$ column densities of them are not significantly different. We also discuss the observational effects, such as those induced by the finite spatial resolution, beam dilution and line-of-sight projection, on the morphological classification of molecular clouds in our sample.

## 46. Global 3D Radiation Hydrodynamic Simulations of Proto-Jupiter's Convective Envelope

**Zhaohuan Zhu, Yan-Fei Jiang, Hans Baehr, Andrew N. Youdin, Philip J. Armitage, Rebecca G. Martin** ★ The core accretion model of giant planet formation has been challenged by the discovery of recycling flows between the planetary envelope and the disc that can slow or stall envelope accretion. We carry out 3D radiation hydrodynamic simulations with an updated opacity compilation to model the proto-Jupiter's envelope. To isolate the 3D effects of convection and recycling, we simulate both isolated spherical envelopes and envelopes embedded in discs. The envelopes are heated at given rates to achieve steady states, enabling comparisons with 1D models. We vary envelope properties to obtain both radiative and convective solutions. Using a passive scalar, we observe significant mass recycling on the orbital timescale. For a radiative envelope, recycling can only penetrate from the disc surface until $\sim$0.1-0.2 planetary Hill radii, while for a convective envelope, the convective motion can "dredge up" the deeper part of the envelope so that the entire convective envelope is recycled efficiently. This recycling, however, has only limited effects on the envelopes' thermal structure. The radiative envelope embedded in the disc has identical structure as the isolated envelope. The convective envelope has a slightly higher density when it is embedded in the disc. We introduce a modified 1D approach which can fully reproduce our 3D simulations. With our updated opacity and 1D model, we recompute Jupiter's envelope accretion with a 10 $M_\oplus$ core, and the timescale to runaway accretion is shorter than the disc lifetime as in prior studies. Finally, we discuss the implications of the efficient recycling on the observed chemical abundances of the planetary atmosphere (especially for super-Earths and mini-Neptunes).

## 47. The HD 98800 quadruple pre-main sequence system. Towards full orbital characterisation using long-baseline infrared interferometry

**S. Zúñiga-Fernández, J. Olofsson, A. Bayo, X. Haubois, J. M. Corral-Santana, A. Lopera-Mejía, M. P. Ronco, A. Tokovinin, A. Gallenne, G. M. Kennedy, J. -P. Berger** ★ HD 98800 is a young ($\sim$ 10 Myr old) and nearby ($\sim$ 45 pc) quadruple system, composed of two spectroscopic binaries orbiting around each other (AaAb and BaBb), with a gas-rich disk in polar configuration around BaBb. While the orbital parameters of BaBb and AB are relatively well constrained, this is not the case for AaAb. A full characterisation of this quadruple system can provide insights on the formation of such a complex system. The goal of this work is to determine the orbit of the AaAb subsystem and refine the orbital solution of BaBb using multi-epoch interferometric observations with the VLTI/PIONIER and radial velocities. The PIONIER observations provide relative astrometric positions and flux ratios for both AaAa and BaBb subsystems. Combining the astrometric points with radial velocity measurements, we determine the orbital parameters of both subsystems. We refined the orbital solution of BaBb and derived, for the first time, the full orbital

solution of AaAb. We confirmed the polar configuration of the circumbinary disk around BaBb. From our solutions, we also inferred the dynamical masses of AaAb ($M_{Aa} = 0.93 \pm 0.09$ and $M_{Ab} = 0.29 \pm 0.02$ $M_\odot$). We also revisited the parameters of the AB outer orbit. Using the N-body simulation, we show that the system should be dynamically stable over thousands of orbital periods and that it made preliminary predictions for the transit of the disk in front of AaAb which is estimated to start around 2026. We discuss the lack of a disk around AaAb, which can be explained by the larger X-ray luminosity of AaAb, promoting faster photo-evaporation of the disk. High-resolution infrared spectroscopic observations would provide radial velocities of Aa and Ab (blended lines in contemporary observations), which would allow us to calculate the dynamical masses of Aa and Ab independently of the parallax of BaBb.